UNIVERSITY OF TWENTE

Faculty of Science and Technology
Chemical Process Engineering
Soft Matter, Fluidics and Interfaces

Mass Transfer in Titania Photocatalytic Membrane Reactors

Danny Dijkhuis

Examination Committee:
Prof. Dr. Ir. R.G.H. Lammertink
Prof. Dr. G. Mul
MSc. A. Visan
July 13, 2017

Abstract

This report presents a mass transfer model for plasma oxidized TiO_2 membranes in a dead-end photocatalytic membrane filtration module. The model takes into account several parameters such as membrane dimensions, porosity, a first order reaction and convective and diffusive mass transfer. Experimental data was acquired for several different membrane dimension and flowrates. By applying the experimental data on the mass transfer model unkown parameters could be calculated. When having exact dimensions and porosity of a membrane, the model is capable to predict the eventual concentration and concentration polarization effects. With help of the mass transfer model, a sensitivity analysis was made to describe the impact of several parameters on the degredation and concentration polarization. By fitting the experimental data, a reaction rate constant in the order of $10^{-2}s^{-1}$ was acquired. With a methylene blue degradation of up to 84% and relative low trans membrane pressures below 1 bar, plasma oxidized membranes have shown great potential for possible future applications.

Contents

1 Introduction

Increasing shortage of clean water sources worldwide inspires the development towards low-cost and high efficiency water purification technologies. High water quality is a big responsibility for companies in the water industry due to increasing environmental standards as well as emerging contaminants such as persistent organic pollutants and hormones. Furthermore, some conventional water treatment processes involve the addition of chemicals to turn suspended solids into sludge that produces a significant amount of solid waste and leads to secondary waste problems. The past decades have shown significant progress towards effective processes to remove various pollutants in wastewater. [1, 2] This research will focus on wastewater treatment by using a photocatalytic membrane reactor, combining membrane filtration with photocatalysis.

1.1 Photocatalysis

Research has been done towards water and wastewater treatment, via advanced oxidation using semiconductor photocatalysis. TiO_2 [3–6], Fe_2O_3 [7], ZnO [8], several others and their compositites have been investigated as semiconductors for photocatalysis. Among these photocatalysts, titanium dioxide (TiO_2) is the most appealing photocatalyst, as it is chemically stable, inexpensive, non-toxic and commercially available. [3–6]

There are three metastable phases for TiO_2, known as rutile, anatase and brookite. The anatase phase has a bandgap energy of 3.23 eV (384 nm), where the energy of the rutile phase is equal to 3.02 eV (411 nm). This makes the anatase phase desirable for photocatalysis, due to its ability to excite the bandgap of UV-light. [9–13] The photon energy of UV light, hv, which illuminates TiO_2 exceeds the bandgap of 3.23 eV. Thus, absorption of the photon by TiO_2 excites an electron (e^-) from the valance band to the conduction band, which leads to an electron gap, h^+, in the valance band as shown in Eq.(1) [3, 14] The excited electron and electron gap then migrate to the surface of TiO_2 where they participate

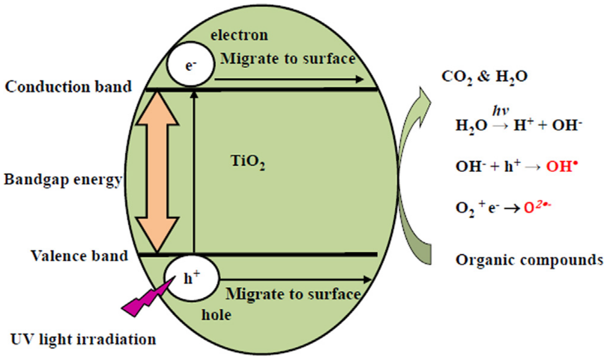

Figure 1.1: Schematic overview of photocatalytic degradation using TiO2 [3]

in a series of redox reactions, as schematically depicted in Figure 1.1. The electrons will reduce titanium (IV) to titanium (III) (Eq.(2)), whereas titanium(III) will react with absorbed oxygen on the titanium surface to form superoxide radical anions in an aerated aqueous system (Eq.(3)).The electron gap (h^+) reacts with water molecules, which are absorbed on the TiO_2 surface, to form hydroxyl radicals ($OH^\bullet$), Eq.(4). Organic pollutants (R) in wastewater can be oxidized by the reactive radicals and superoxide radical anions to carbon dioxide and water, Eq.(5) and Eq.(6). Both radicals can also inactivate microorganisms, bacteria and viruses.

$$\mathrm{TiO_2 + hv \longrightarrow e^- + h^+} \tag{1}$$

$$\mathrm{Ti(IV) + e^- \longrightarrow Ti(III)} \tag{2}$$

$$\mathrm{Ti(III) + O_2 \longrightarrow Ti(IV) + O_2{}^{\bullet -}} \tag{3}$$

$$\mathrm{H_2O + h^+ \longrightarrow OH^\bullet + H^+} \tag{4}$$

$$\mathrm{OH^\bullet + R \longrightarrow intermediates \longrightarrow H_2O + CO_2} \tag{5}$$

$$\mathrm{O_2{}^{\bullet -} + R \longrightarrow intermediates \longrightarrow H_2O + CO_2} \tag{6}$$

The amount of light penetration to the catalyst surface, the duration of light irradiation, the surface area of the catalyst and the initial concentration of the pollutant all affect the efficiency of TiO_2 as a photocatalyst. A key factor is the surface area of the catalyst in catalytic reactions. Photocatalysts based on TiO_2 have shown high photocatalytic efficiency for large surface areas, and thus nano-sized particles TiO_2 were used in most studies. For homogeneous reactions, results have shown that nano-sized TiO_2 outperforms its bulk counterparts. [15]

1.2 Membrane filtration

Membrane processes have become one of the most effective technologies for water treatment in the past decades due to their small footprint, easy maintenance, separation efficiency and their ability to scale up easily. However, membrane filtration traditionally results in accumulation of retained species at the membrane surface interface, a phenomena known as concentration polarization and membrane fouling. Concentration polarization and fouling cause a limiting flux because the permeation rate of the membrane will be balanced by back-diffusion. Increased pressures will no longer result in a significant increase in flux as the accumulation layer keeps growing.

There are several driving forces for membrane processes, which can be pressure difference, concentration difference, partial pressure difference or electrical potential difference. Based on the driving forces, different groups of membranes can be distinguished. Pressure driven membrane processes can be separated into microfiltration, ultrafiltration, nanofiltration and reverse osmosis. The solvent and various solute molecules will permeate through the membrane, whereas other molecules or particles can be (partly) rejected dependening on the structure of the membrane. Pressure driven membranes can be distinguished by pore size, where microfiltration has the largest pores and reverse osmosis has the smallest. Smaller pore sizes result in a larger mass transfer resistance. Hence, the applied pressure must be increased to maintain the same flux. [16]

Membrane filtration can be executed in either a dead-end mode or cross-flow mode. The dead-end mode will let the entire feed pass through the membrane to become a filtrate. This results in increasing concentration of the separated substance which will eventually lead to a cake layer and concentration polarization on the membrane surface. Both the cake layer and concentration polarization will reduce the effectiveness and flux of the membrane. At first this can be resolved by increasing the pressure. However, after a certain accumulation of retained species on the membrane surface, pressure increases will no longer change the membrane flux significantly. Therefore, dead-end filtration is mainly used in smaller processes while it is unsuitable for large-scale processes. In cross flow, the feed solution on the upstream side of the membrane moves parallel to the membrane and the permeate will through the membrane. The retentate can be recycled to the feed. The advantage of cross flow configuration over dead-end mode is the removal of fouling along with the retentate stream.

1.2.1 Resistance model

The permeate flux through a porous membrane is often described as the applied transmembrane pressure driving force, ΔP in Pa, divided by the total membrane resistance, R_{tot} in m^{-1}, and the permeate viscosity, μ in Pas, leading to Eq.(7) [17–19] and Figure 1.2. This is also called the resistance model.

$$J = \frac{\Delta P}{Rtot\mu} \tag{7}$$

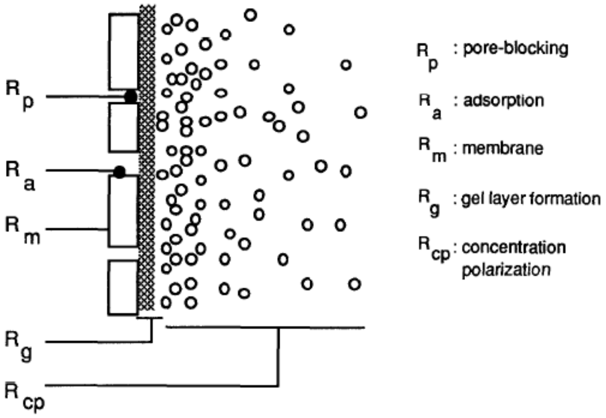

Figure 1.2: Possible resistances against solvent transport [19]

An important reason why membrane processes are not used in large scale is the flux decline during membrane filtration. Flux decline can be caused by several phenomena in the bulk, in the membrane or on the membrane surface. The so-called critical flux or clean water flux is the maximum flux which can be achieved with only negligible fouling. The exact value of critical flux can depend on foulant properties, membrane properties and local velocity. [20]. Flux decline is generally caused by a decreased driving force or increased resistance. Controlling the flux however, will lead to an increased driving due to an increased resistance. All resistances except for Rm, which is the intrinsic membrane resistance and thus always present, can develop during the process. An increased resistance can occur because pores are being blocked by the solute (R_p). Even so, adsorption of the solute onto walls of the pores will lead to an increased resistance, hence a less permeable membrane (R_a). A very important phenomenon for this research is concentration polarization. Due to the membrane retaining species while letting the solvent pass through, the solute will accumulate at and near the membrane surface with a relatively high concentration. Compared to an unaltered solution, the solvent undergoes an additional resistance due to the concentrated layer of solute (R_{cp}). For extremely high concentration polarization processes, such as reverse osmosis, the concentrated layer can reach such high values that the concentrated solution will change into a gel layer (R_g). [19]

1.2.2 Concentration Polarization

The increasing layer of solute near the membrane interface can be described as cake-filtration or by the film theory. For this research the focus is mainly on the film theory, which is depicted in Figure 1.3. Generally, the film theory is described

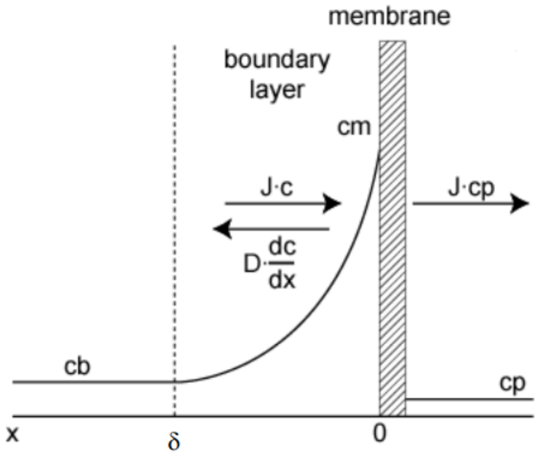

Figure 1.3: The film theory to described concentration polarization

by Equation 8.

$$\frac{dC}{dt} + J\frac{dC}{dx} = D\frac{d^2C}{dx^2} \tag{8}$$

where $J\frac{dC}{dx}$ represents the convective transport towards the membrane, while $D\frac{d^2C}{dx^2}$ describes the back-diffusion as a result of the gradient in concentration.

1.3 Photocatalytic membrane reactors

Hybrid processes combining membrane separation and heterogeneous photocatalysis are generally referred to as photocatalytic membrane reactors, PMRs have shown great potential for usage in water purification and water treatment processes, because the combination of photocatalysis and membrane filtration endorse each others advantages while subsequently reducing their negative traits. [3, 21] Photocatalytic membrane reactors can be split into two main catogories as shown in Figure 1.4, which have different configurations for themselves. Firstly there are slurry photocatalytic membrane reactors (a), which have a catalyst suspended in the reaction mixture. Secondly there are reactors with a catalyst immobilized in or on the membrane. [16, 22, 23]

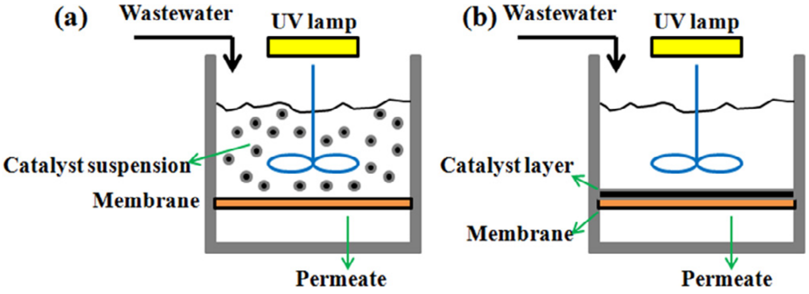

Figure 1.4: Categories of photocatalytic membrane reactors. (a) Slurry reactor, where the catalyst is suspended in the reaction mixture and (b) Immobilized PMR, where the catalyst is immobilized in or on the membrane [22]

PMRs have several advantages over conventional photocatalytic reactors such as reducing the loss of photocatalyst in the reaction bulk, controlling the residence time in the reactor and realizing a continuous process with simultaneous separation of catalyst and products. [24] This leads to improved process effeciency and stability as well as being able to reuse the photocatalyst to reduce operating costs. [22]

1.3.1 PMRs configurations

Currently, the two main categories of PMRs can be split into four different configurations of integrated water treatment processes by combining photocatalytic oxidation and membrane filtration. The different configurations are described as a slurry photocatalytic reactor followed by a membrane filtration unit, inorganic or polymeric membrane submerged in a photocatalytic reactor, a membrane placed inside a photoreactor whose internal walls are coated by a photocatalyst and a photocatalytic membrane such as a pure TiO_2 porous membrane or a TiO_2 composite membrane. [3,16]

Out of these configurations the photocatalytic membrane has an advantage over the other configurations since it combines the physical separation of membrane filtration and the organic degradation by for example TiO_2, achieved by photocatalysis in a single unit. It is expected TiO_2 photocatalytic membranes can reduce concentration polarization and membrane fouling and additionally improve permeate qualities.

1.4 TiO_2 photocatalytic membranes

Photocatalytic TiO_2 membranes can be split in two categories: immobilized TiO_2 membranes on a support and a pure porous TiO_2 membranes. Many materials have been used as supports for the fabrication of immobilized photocatalytic membranes including metallic, organic and inorganic materials. In most cases, polymer and ceramic membranes are used as supports for TiO_2 photocatalytic membranes like Al_2O_3 [9,25], polysulfone [26], poly(vinylidene fluoride) [27], polyurethane [28] and many others [3].

Other than immobilized photocatalytic membranes, some research has been done onr pure TiO_2 porous membranes. These pure porous TiO_2 membranes have been fabricated by using nanotubes [29], nanofibers [30] or nanowires [31].

1.4.1 Reaction kinetics

The reaction kinetics for photocatalytic reactions are important to determine the rate of degradation for pollutants. Recent research shows that most of the degradation reactions by a TiO_2 photocatalytic membrane use pseudo-first order kinetics, regardless of the type of pollutant. [9,10,27,28,30,32–36] See Equation 9.

$$-\frac{dC}{dt} = R \tag{9}$$

This is equation holds for plug flow reactors when neglectic mass transfer limitations.

Equation 10 is the governing equation for fluid motion of species. In this research Equation 10 will be used as a base for describing the mass transfer and reaction rate in photocatalytic membranes, as described in more detail in Chapter 3.4.

$$D\frac{d^2C}{dx^2} = u\frac{dC}{dx} + kC \tag{10}$$

1.5 Application of TiO_2 photocatalytic membranes

A significant amount of research towards TiO_2 photocatalytic menbrabe reactors has been devoted to applications in wastewater treatment and water purification. [9,30,31,34,36,37] In water treatment applications it is important to find an optimal balance between the photocatalytic activity and membrane flux in order to achieve the best overall performance. The pollutant mostly used to model organic pollutant removal has been methylene blue [11, 30, 38–40]. Besides methylene blue, methyl orange [10, 12, 35, 40–42], direct black 168 [9], reactive black 5 [27, 32, 33] and many others have been used.

Besides water treatment, photocatalytic membranes are extensively studied on their anti-bactericidal effects where E. coli was mostly used as an indicator [25, 26, 30, 33, 39, 43].

2 Scope of research

This research will focus on several photocatalytic porous membranes existing of pure TiO_2 or an α-Al_2O_3 supported membrane with a layer of TiO_2. The main focus will be on the pure TiO_2 membranes, as they generally outperform traditional membranes due to reduced membrane fouling and additionally improved permeate qualities. It is expected a membrane with a catalysed layer or consisting of pure TiO_2 will reduce the effects of concentration polarization due to degradation of species near the membrane surface. Firstly, a 1D model in dead-end mode is created, where parameters such as, membrane porosity, membrance thickness, membrane surface area, flowrate and reaction rate are implemented. All these parameters can possibly influence the performance of the photocatalytic membrane. Next there will be made an experimental setup, which allows comparison between the theoretical mass transfer model and experimental results. Finally, this should lead to a model that can predict the concentration profile and effectiveness of the photocatalytic membrane and it will also be used to generate a sensitivity analysis for most parameters.

3 Methods

3.1 Experimental Setup

The setup of the photocatalytic membrane reactor is schematically shown in Figure 3.1. A helium filled gas cylinder operating at 10 bar is connected to the feed containing the solution in order to pressurize the feed, with several safety valves in between. The solution will then pass a flow controller and a pressure indicator which are connected to a convergence inspector, that on its turn is connected to a computer where the flow can be controlled and the pressure can be measured. The solution will then enter the photocatalytic membrane reactor module, where the permeate is led to a sample analysis done in an Ocean Optics minispectrometer, which is also connected to the computer where absorption and therefore concentration can be measured. The membrane module is irridiated by two UV light source fibers connected to a HP120 UV-elektronik device.

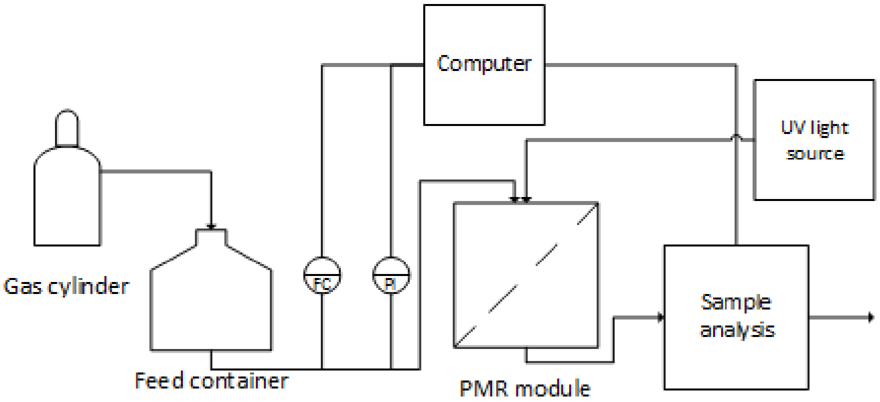

Figure 3.1: Schematic overview of experimental setup

3.1.1 Spectrometer calibration

The Ocean Optics minispectrometer has to be calibrated to transform absorption to a concentration. The concentrations used for calibration are 30, 20, 10, 5, 2 and 1 μM of methylene blue, resulting in a Concentration vs. Absorbance graph. Where the concentration can be determined by taking the absorption from the spectrometer and finding the corresponding concentration. Figure 3.2 shows the result for calibration. The first calibration was done cleaning the spectrometer in between different concentrations (cleaning, the second calibration was done without cleaning in between, starting with the highest concentration of 30 μM methyleneblue (No-cleaning). Remarkably, at lower concentrations there is a significant difference between the cleaned and non-cleaned calibration. Since the setup is a closed system, which has an inability to clean the spectrometer during the experiment, the actual concentration has to be adjusted accordingly.

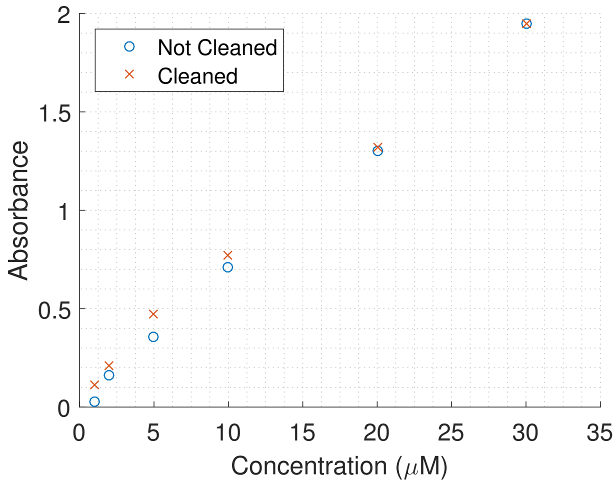

Figure 3.2: Calibration of spectrometer, comparing cleaning with no-cleaning

3.1.2 Photocatalytic membrane reactor module

The photocatalytic membrane reactor is depicted in Figure 3.3. It ressembles a dead-end photocatlatic membrane filtration reactor. The solution will flow from the inlet (top) to the reaction chamber, where the membrane surface is irridiated by UV-light, hence a photocatalytic reaction combined with filtration occurs once the system is pressurized. The UV-light fibers irridiate the chamber under an angle of 45°, which is enough to distribute the light over the entire active surface of the membrane. The module is closed off tightly by screws which connect the top and bottom part of the module, with O-rings to fill the gap between the membrane and the module. The module is made to withstand pressures which are significantly higher than the pressure required for filtration. The module was created in cooperation with the TCO (Techno Centrum voor Onderzoek en Onderwijs) department of the University of Twente.

3.2 Experimental

Clean water experiments were prepared by filling the feed container with milli-Q water and inserting the membrane in the PMR-module. The UV-light source was kept off during these experiments. Once preparation was completed, the feed was controlled by the convergeance inspector at a constant rate. The experiments ran untill shifts in pressure were no longer observed.

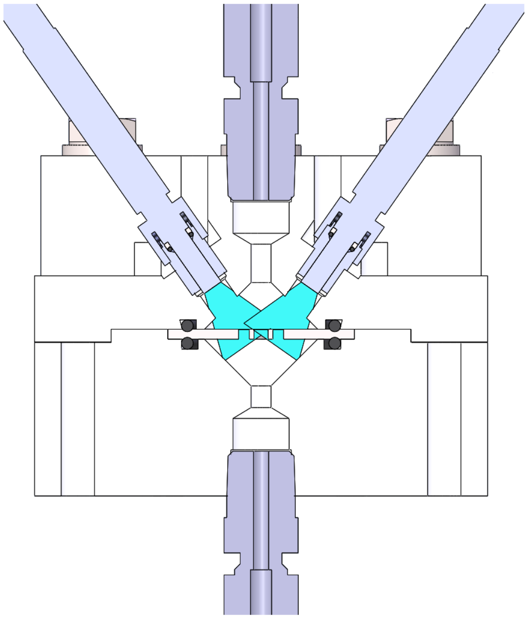

Figure 3.3: Schematic drawing of the photocatalytic membrane module

Experiments to measure pressure increase over time for general dead-end membrane filtration were conducted by filling the feed container with a 5 or 10 μM methylene blue solution. The entire setup was first filled with the solution, which results in a value for adsorption of the base concentration. When the adsorption of the bulk concentration was aqcuired, the module was opened and the membrane inserted. Then the feed was controlled at a constant rate. The experiments were stopped when either the membrane reached its pressure limit or when the pressure came close to limits of previous experiments.
The irridiated experiments were achieved by filling the system with a 5 or 10 μM methylene blue solution. Once the system was filled, the adsorption of the bulk concentration was determined. The membrane was inserted by opening the module. Once the membrane was inserted the UV-light was turned on, and the feed was controlled at low flowrates between 0.1 and 1 g/hr for different experiments.

3.3 Membrane preparation

Three different TiO_2 photocatalytic membranes will be used for the experiments, a pure Tio_2 porous membrane manufactured by the company Metal Membranes located in Leeuwarden, The Netherlands, a layer of TiO_2 was created by using the electrospinning process on a alumina support and an alumina membrane where titania is deposited on the surface.

3.3.1 Pure TiO_2 membranes by plasma electrolytic oxidation

Metal Membranes has developed a way to make porous ceramic membranes from alumina or titania. The technique to create these membranes consists of two steps. The first step is to create a porous ceramic layer, which is done using a process called plasma oxidation. Plasma electrolytic oxidation processing is a well-known industrial surface treatment for light metals offering a reasonable wear and corrosion protection. The process is derived from conventional anodizing to form ceramic-like coatings, but it employs higher potentials, so discharges occur and the resulting plasma modifies the structure of the oxide layer. The process can be used to grow large crystalline, oxide coatings on metals. [44] When using the right conditions, a porous ceramic layer can be formed on titanium, which can be used as a photocatalytic membrane. A work plate, made from either aluminium or titanium is placed in the machine. A cathode is then positioned on top of the work plate, leaving a small gap for processing. The process gap is then filled with saline water, and a high voltage field is created between the metal plate and the cathode. The high voltage field creates a plasma, which transforms the metal surface layer into ceramic. Depending on the conditions within the process gap, different types of ceramic can be created. Once the plasma oxidation is completed, one side is ceramic while the other is still a solid metal. The second step is a process called electrochemical machining.

Through the use of chemistry and electricity the metal dissolves quickly and accurately until the ceramic layer is reached. Leaving a porous ceramic layer which is still connected to the metal, creating a membrane. The metal plate used for this process is titanium with a diameter of 28 mm and thickness of 1 mm. The ceramic layer created by plasma oxidation has a diameter of 20 mm, a thickness of 20-80 μm and a porosity of 20-80%. The metal removed on the backside of the metal plate can be modified accordingly. Schematic drawings of the top and bottom side of such a metal membrane can be found in Figures 3.4 and 3.5.

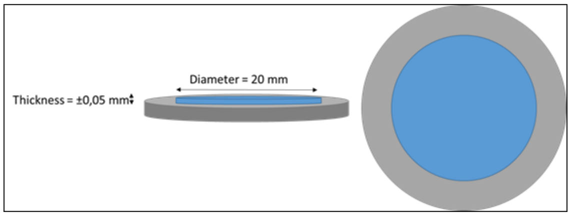

Figure 3.4: Schematic drawing top side of a plasma oxidized membrane

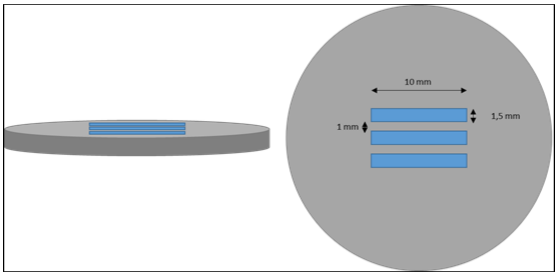

Figure 3.5: Schematic drawing bottom side of a plasma oxidized membrane

3.3.2 TiO_2 deposited by electrospinning on an alumina support

TiO_2 nanofibers can be fabricated by use of electrospinning. [28] Electrospinning is a relatively simple method for generating fibular mesostructures. In typical processes, a solution containing polymers or melt is injected under the influence of an electric field. Electrospinning shares characteristics of conventional dry spinning and electrospraying of fibers. When a sufficiently high voltage is applied to a liquid, it becomes charged, and the surface tension is then countered by electrostatic repulsion and the droplet is stretched which leads to a stream of liquid from the surface. If the stream is not interrupted, a charged liquid jet is formed to assure that the molecular cohesion of the liquid is sufficiently high. The jet will then dry in flight, the current flow will change from ohmic to convective as the charge migrates to the surface. The jet is elongated by electrostatic repulsion, initiated at small bends in the fiber. The elongation and thinning of the fiber resulting from the bending instability leads to the formation of uniform fibers with diameters in the order of nanometers [45, 46]. A schematic overview of an electrospinning setup is depicted in Figure 3.6.

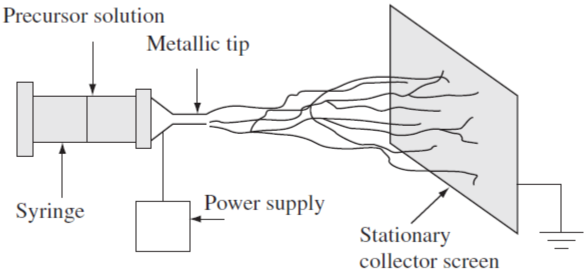

Figure 3.6: A schematic overview of a electrospinning setup [47]

Prior to electrospinning, a solution was prepared. Starting with a titanium alkoxide, and in this specific case titianium(IV) ethoxide which has the formula $Ti(OCH_2CH_3)_4$, a molecular weight of 228,11 g/mol and a density of 1,088 g/cm^3.

The titanium alkoxide was dissolved in 2-methylethanol to create a 1 M solution. To make a solution with a total volume of 10 ml, it required 2,097 ml of titanium(IV) ethoxide and 7,903 ml 2-methylethanol which was done in a vacuum glove box.
The 1 M alkoxide solution was then mixed with acetic acid and water in a volume ratio of 1000:215:85, respectively in the stated order. Followed by mixing the precursor with chloroform in a 85:15 volume ratio and 10 $\mu g/ml$ PVP (Polyvinylpyrrolidon). The solution was then stirred for several hours to ensure complete dissolution.

The solution was then inserted into a syringe and set to flow at 0.01 g/hr with a syringe pump. A distance of 20 cm between the collector screen (an α-AL_2O_3 membrane) and the metallic tip was maintained. And an electric field of 20 kV was applied to the collector screen. The experiment ran for a total duration of 1 hour. The α-Al_2O_3 support with a layer of TiO_2 was then sintered for 2 h at 500 °C in air with heating and cooling steps of 2 °C/min , which was done with comperable solutions by Visan et al. [48] and Aran et al. [49].

3.3.3 Dip coating of TiO_2 on an alumina membrane

Dip-coating is a widely studied method immobilization method for fabricating photocatalytic ceramic membranes. [9, 11, 12, 25, 38–41, 49, 50] Basically, dip coating is the withdrawal of a substrate from a fluidic solution or dipping the top layer of a substrate in a solution while attached to a vacuum pump. When the dipping is completed; gravitational draining, solvent evaporation and further condensation reactions result in the depostion of a solid film on the substrate. When this is completed, the membrane is generally sintered to evaporate the solvent and increase the cohesion of the layer to the surface. [51]

For this experiment, a α-Al_2O_3 support is used, with a thickness of 2mm and a diameter of 38mm. The solution was prepared by diluting Evonik, VP Disp. W2730, which has a pH of 6.0-8.0, a density of 1.28 g/cm^3, mean aggregate size of 100 nm, TiO_2 content of 29 - 31 % and a viscosity of ¡5000 $mPas$. The precursor is the diluted 30 times with water. When the Evonik precursor is diluted, the fraction of TiO_2 is reduced to 0.01. The solution was put into a petri dish, while the substrate was attached to a holder by vacuum. The holder makes a circular motion, thus it is necessary the height of the petri dish is adjusted accordingly. This is followed by a singular automated clockwise motion of the holder, where only the top part of the support gets in contact with the solution. Like in the electrospinning process, after sol dipping, the α-Al_2O_3 support with a layer of TiO_2 was then sintered for 2 h at 500 °C in air with heating and cooling steps of 2 °C/min.

3.4 Mass transfer model

Modelling the photocatalytic membrane will be split into two regions; a region before the membrane and the membrane itself. It is assumed the filtration happens at the surface of the membrane. Thus the model will be ranging from $x = -L_1$ to $x = L_2$, where $x = -L_1$ is the start of the mass transfer boundary layer and

$x = L_2$ is the end of the membrane.

Region 1: Bulk zone without reaction, extending from $x = -L_1$ to $x = 0$.
Region 2: Reactive zone, extending from $x = 0$ to $x = L_2$.

The mass transfer in the first region will only depend on a convective and diffusive term, which leads to Eq.(11). The second region will be affected by both convection and diffusion as well as a chemical reaction, which leads to the differential equation described in Eq.(12).

$$D_1 \frac{d^2 C_1}{dx^2} = u_1 \frac{dC_1}{dx} \qquad \text{for } (-L_1 < x < 0) \tag{11}$$

$$D_2 \frac{d^2 C_2}{dx^2} = u_2 \frac{dC_2}{dx} + kC_2 \qquad \text{for } (0 < x < L_2) \tag{12}$$

Where D_i is the diffusion coefficient (m^2/s), u_i the local flow velocity (m/s), C_i the concentration $(mole)$, k the reaction rate constant (s^{-1}) and x the axial coordinate (m). The membrane will have different constants for both D and u compared to the bulk, $D_2 = D_1 \epsilon$ and $u_2 = u_1/\epsilon$. The equations (11) and (12) can be made dimensionless by introducing a dimensionless axial coordinate $X = x/L_2$ and a second Dahmkohler number for the source term $K = \frac{kL^2}{D_2}$, then taking all constants to one side will result into Eq.(13), where the final constant, $\frac{u_i L_i}{D_i}$ is equal to the Peclet (Pe_i) number. By introducing the axial dimensionless coordinate, the dimensionless source term and the difference in Pe_i number for regions 1 and 2, the equations (11) and (12) can be rewritten to equations (14) and 15).

$$\frac{d^2 C_i}{dX^2} = \frac{u_i L_i}{D_i} \frac{dC_i}{dX} \tag{13}$$

$$\frac{d^2 C_1}{dX^2} = Pe_1 \frac{dC_1}{dX} \qquad \text{for } (-L_1 < X < 0) \tag{14}$$

$$\frac{d^2 C_1}{dX^2} = Pe_2 \frac{dC_2}{dX} + KC_2 \qquad \text{for } (0 < X < L_2) \tag{15}$$

Where $Pe_1 = \frac{u_1 L_2}{D_1}$ and $Pe_2 = \frac{u_2 L_2}{D_2}$. To solve these equations, dimensionless boundary conditions are required. Therefore, the regions have to be made dimensionless. L_2 will be normalized to 1, which is the thickness of the membrane, and L_1 will be considered B where $-B = L_1/L_2$. The concentration at B is equal to the inlet concentration, which is normalized to 1. The boundaries between both regions are the concentration of the second region multiplied by a retention factor (α) and the continuity in fluxes.

The dimensionless boundary conditions for the flux will require a slight alteration where D_i is divided by the length of the region (L_1 and L_2). Finally, the boundary condition at the end of the membrane states the concentration is finite, thus $\frac{dC}{dX} = 0$. Hence, the two second order differential equations (14) and (15) are subject to the dimensionless boundary conditions described in equations (16) to

(19).

$$\text{B.C.1} \qquad C_1 = 1 \qquad \text{at } X = -B \qquad (16)$$

$$\text{B.C.2} \qquad C_1 = C_2\alpha \qquad \text{at } X = 0 \qquad (17)$$

$$\text{B.C.3} \qquad \frac{D_1}{L_1}\frac{dC_1}{dX} - u_1C_1 = \frac{D_2}{L_2}\frac{dC_2}{dX} - u_2C_2 \qquad \text{at } X = 0 \qquad (18)$$

$$\text{B.C.4} \qquad \frac{dC_2}{dX} = 0 \qquad \text{at } X = 1 \qquad (19)$$

Solving the differential equations (14) and (15) will lead to the following indefinite integrals:

$$C_1(X) = A_1 + A_2e^{Pe_1X} \qquad \text{for } -B < X < 0 \qquad (20)$$

$$C_2(X) = A_3e^{m_+X} + A_4e^{m_-X} \qquad \text{for } 0 < X < 1 \qquad (21)$$

Where $m_+ = \frac{1}{2}(Pe_2 + \sqrt{Pe_2^2 4K})$ and $m_- = \frac{1}{2}(Pe_2 - \sqrt{Pe_2^2 4K})$
In order to solve the integration constants A_{1-4}, the boundary conditions have to be implemented. There are four unknowns, and four possible equations when combining them with $B.C._{1-4}$ which means a solution can be found by making a set of linear equations. By filling in the boundary conditions of equations (16) to (19) for equations (20) and (21) will lead to the following set of linear equations;

$$A_1 + A_2e^{Pe_1-B} = 1 \qquad (22)$$

$$A_1 + A_2 - (A_3 + A_4)\alpha = 0 \qquad (23)$$

$$\frac{D_1}{L_1}Pe_1A_2 - u_1(A_1 + A_2) - \frac{D_2}{L_2}(m_+A_3 + m_-A_4) + u_2(A_3 + A_4) = 0 \qquad (24)$$

$$m_+A_3e^{m_+} + m_-A_4e^{m_-} = 0 \qquad (25)$$

The equations (22) to (25) are implemented in a Matlab code, as described in Appendix A.1, where the integration constants are calculated.

By using the calculated integration constants in equations 20 and 21, the concentration profile can be solved. The Matlab code which is used to acquire the concentration profile can be found in Appendix A.2. To check the model, three base cases have been created and investigated. For all cases, diffusion, velocity, membrane thickness and the boundary mass transfer layer are equal. The first case represents the model of only a membrane and no reaction (Figure 3.7). As expected this leads to an increase of concentration at the membrane surface. The second case represents a model of a reactive layer without filtration (Figure 3.8). Expectations of these settings are met by leading to a concentration profile which starts degradation close to the membrane surface until the end of the membrane. The final case represents the model where membrane filtration and photocatalytic reaction are combined, where the reactive part should reduce the concentration polarization (Figure 3.9).

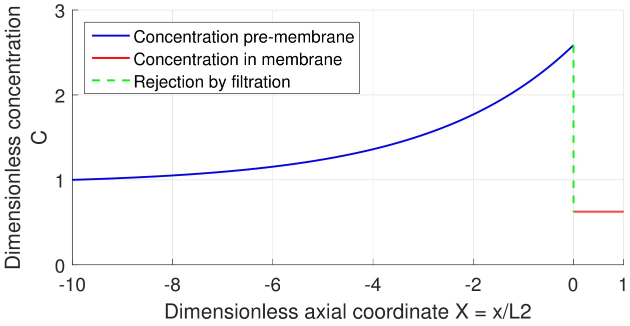

Figure 3.7: Concentration profile of a model with only membrane filtration. Flowrate = 0.2 g/hr, Porosity = 0.5, Membrane diameter = 4 mm, Membrane thickness = 65μm ,α = 5 and k = 0

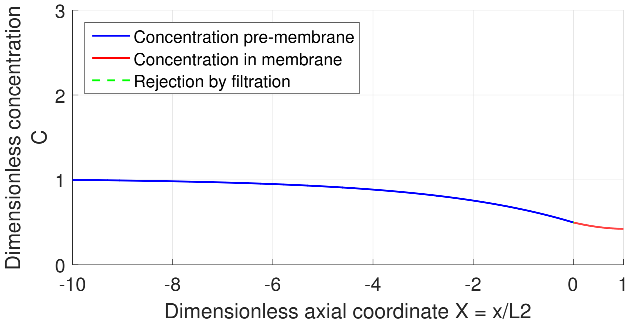

Figure 3.8: Concentration profile of a model with only reaction. Flowrate = 0.2 g/hr, Porosity = 1, Membrane diameter = 4 mm, Membrane thickness = 65μm ,α = 1 and k = 0.065

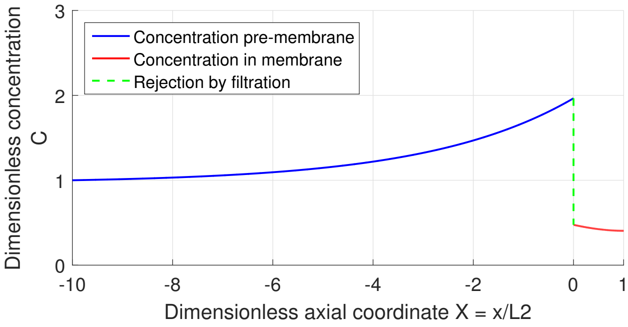

Figure 3.9: Concentration profile of a model with both reaction and filtration. Flowrate = 0.2 g/hr, Porosity = 0.5, Membrane diameter = 4 mm, Membrane thickness = $65 \mu m$, $\alpha = 5$ and k = 0.065

3.4.1 Defining modelling parameters

In order to use the mass transfer model described in Chapter 3.4, several parameters have to be defined.

Flux

The flux pre-membrane and in the membrane are defined by using the flowrate, area and porosity. Equations 26 and 27 describe the two fluxes required for the mass transfer model.

$$u_1 = \frac{F\frac{1e-6}{3600}}{A_m} \tag{26}$$

$$u_2 = \frac{F\frac{1e-6}{3600}}{A_m \epsilon} \tag{27}$$

Where F is the flowrate in g/hr, A_m is the membrane surface area in m^2 and ϵ the porosity of the membrane. For Equation 27 it is assumed the pores of the membranes are cylindrical, thus it increases the velocity in the membrane reversibly with the porosity.

Diffusion

For the pre-membrane region the general value for diffusion of methylene blue in water is taken, which is 5.7e-10 $m^2 s^{-1}$. The diffusivity in the membrane has to be ajusted accordingly. Makhnovskii et al. [52] describe the change in diffusivity in a tube of suddenly alternating diameter. Basically this is also happening inside a membrane, the area which the solution can penetrate reduces linearly with the porosity. Therefore the effective diffusivity in the membrane is calculated according to Equation 28.

$$D_2 = D_1 \epsilon \tag{28}$$

Retention factor

The retention factor α is changing with the CP-modulus. The CP-modulus is described by Equation **??**, whereas α is described by Equation **??**. Both can be found in Chapter 3.4.

Experimentally determined parameters

When the parameters described above are determined, there are still some remaining parameters. These paremeters are; porosity, membrane thickness and the reaction rate constant. These parameters will be determined experimentally.

4 Results and discussion

4.1 α-Al_2O_3 supported membranes

Since there is a significant difference between the α-Al_2O_3 supported and the plasma oxidized membranes, the α-Al_2O_3 supported membranes are examined separately. This is due to the large difference in thickness and the fact that the supported membranes only have a layer of catalyst where the plasma oxidized membranes have the catalyst over the entire membrane.

4.1.1 Electrospun TiO_2 layer

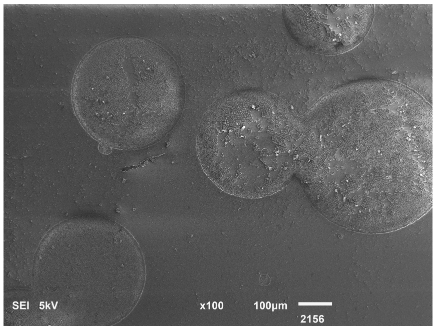

Figure 4.1: TiO_2 layer at 100x magnification

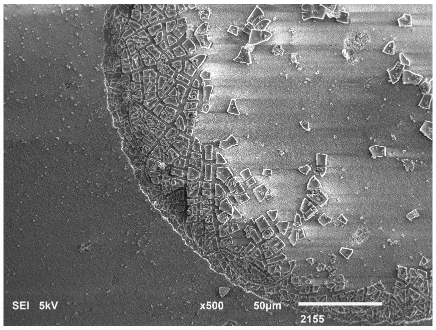

Figure 4.2: TiO_2 layer at 500x magnification

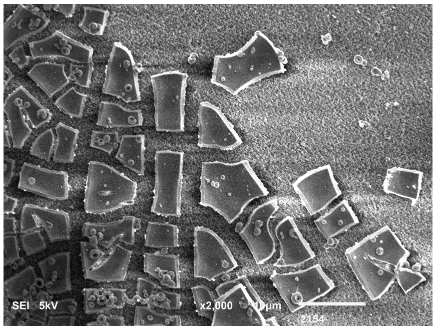

Figure 4.3: TiO_2 layer at 2000x magnification

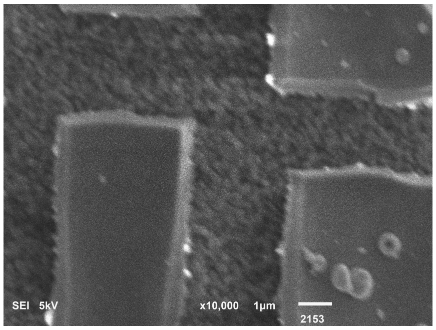

Figure 4.4: TiO_2 layer at 10000x magnification

The electrospun TiO_2 layer, fabricated as described in Chapter 3.3.2, was examined by a scanning electron microscope (SEM). As shown in Figures 4.1 to 4.4, it was unsuccesful to create a uniform TiO_2 catalyst layer on the support. Most ceramic materials are dielectric, which means they have very low electric conductivity but support an electrostatic field. It is very likely TiO_2 deposited in the form of droplets instead of a uniform spun layer by cause of the low electric condictivity of α-Al_2O_3. Seeing that a non-uniform layer has deposited on the support, it was decided to cease the experiments with the electrospun membranes.

4.1.2 Dip coated TiO_2 layer

Dip coating by vacuum was able to create a uniform layer on the α-Al_2O_3 supported membranes. Nevertheless, the supports have a standard diameter of 38mm, whereas the photocatalytic membrane reactor module only supports a diameter of 28mm. Therefore the membranes were cut by laser to 27.9mm so they could fit in the module. Clean water experiments were succesfully conducted with these membranes. When introducing methylene blue however, required trans membrane pressures of about 4 bar appeared to be too high for the membranes. Consequently the membranes were breaking under the pressure and were deemed unworkable for this particular photocatalytic membrane module. Generally the membranes should be able to withstand pressures of up to 5 bar. This implies cutting the mebranes reduced their limits in trans membrane pressure they can withstand due to possible cracks created during laser cutting.

4.2 Intrinsic membrane resistance

The membrane resistance is an intrinsic property of the membrane, and can be considered independent of the driving force. The instrinsic membrane resistance is measured by running the process at a constant flux untill a steady pressure is achieved. Once this pressure is achieved and measured, the intrinsic membrane resistance can be calculated by Eq.(29) [19].

$$J = \frac{\Delta P}{\mu(Rm + Rf)} \tag{29}$$

Where J is the flux in $L/m^2/s$, ΔP the trans membrane pressure in Pa, Rm the hydraulic resistance of the membrane (m^-1), Rf the total resistance of fouling (m^-1), including both concentration polarization and fouling effects on the flux and μ the dynamic viscosity in Pas for an average temperature of 28 °C. Since clean water is used to determine hydraulic resistance of the membrane it is assumed there is no fouling, thus $Rf = 0$. In order to calculate the hydraulic resistance of the membrane Eq.(29) can be rewritten to Eq.(30):

$$Rm = \frac{\Delta P}{\mu J} \tag{30}$$

Both the plasma oxidized and α-Al_2O_3 supported membranes were tested for their intrinsic membrane resistance. All different sized plasma oxidized membranes were used in this experiment, with diameters of 2mm, 3mm, 4mm and a membrane with four seperate areas of 4mm. The α-Al_2O_3 supported membranes all use the maximum size of the membrane module, which is 2cm. The plasma oxidized membranes have a thickness of 50μm, whereas the α-Al_2O_3 supported membranes have a thickness of 2mm.

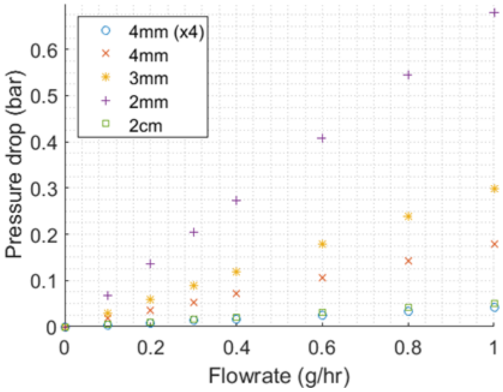

Figure 4.5: Trans membrane pressure versus the flowrate for membranes with different surface areas

As expected and described in Figure 4.5, the membranes show linear pressure increase when increasing the flowrate, this relates to an independent intrinsic membrane resistance for all membranes. According to Equation 30 the plasma oxidized membranes this relates to an intrinsic membrane resistance of 8.97 x 10^9 and 3.10 x 10^{12} for the α-Al_2O_3 supported membranes. This relevant difference in membrane resistances is most likely happening due to the difference in thickness, which is a factor of 400, whereas the factor in resistance is about 346. This means both membrane types would act similar in the case of clean water if their thickness would be equal. However, reducing the thickness of the alumina support 400 times would make it relevantly weaker, making it less resistant to higher pressures.

4.3 Pressure increase

Once the clean water flux is determined, the feed will be switched with a methylene blue solution ranging from 5 to 10 μM. As the experiments are done in dead-end mode, it is expected the pressure will increase rapidly if the surface is not under the effect of irradiation (as the flux would decline rapidly for a constant pressure system). When applying a set flux, the total resistance of fouling can be calculated by fitting the flux, viscosity, intrinsic membrane resistance and measured pressure in Eq.(30). Theoretical flux decline can be calculated reversibly, since the system changes pressure instead of flux to maintain equal fluxes for modelling. A comparison will be made between an irridiated system and a general dead-end membrane system. For an irridiated system, it is expected the system will at some point reach steady state, thus the pressure will no longer increase. Whereas the pressure of a general dead-end membrane is expected to go to infinity.

4.3.1 Dead-end membrane filtration

For general dead-end membrane filtration, the pressure will theoretically increase to infinity. Although, the pressure is limited by the strength of the membrane, which will eventually break under the increasing pressure. Figure 4.6 shows a dead-end membrane filtration with a plasma oxidized membrane with an effective diameter of 2mm, a flowrate of 2 g/hr and a concentration of 10 μM methylene blue. It leads to a close to linear slope for shorter durations, while being exponential for longer experiment durations. After 27 minutes the system had reached a trans membrane pressure of over 0.5 bar, which indicated to be too much for this particular membrane, causing it to break.

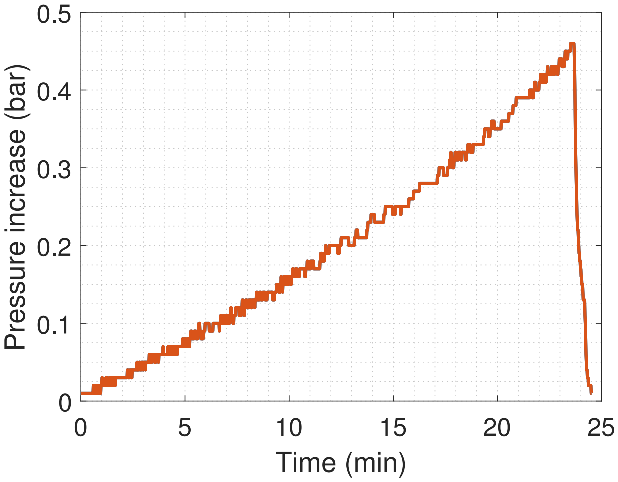

Figure 4.6: Breaking membrane due to pressure increase for a plasma oxidized membrane

4.3.2 Photocatalytic dead-end membrane filtration

For photocatalytic dead-end membrane filtration it is assumed a steady state can be achieved for lower flowrates. Figure 4.7 shows the pressure over time for a photocatalytic dead-end membrane filtration. In this experiment the membrane had an effective diameter of 2mm, the flowrate of the system was 0.2 g/hr and a concentration of 10 μM methylene blue was used. The pressure stabilized after about 7 hours. After 10 hours however, the pressure started to increase slightly. This could be happening either due to deactivation of the catalyst or phenomena of irreversible fouling of the membrane. The peak at 21 hours is most likely an effect of fouling which could be removed afterwards but temporarily increased the resistance. Hence, it increases the pressure for a relatively short period of time. All in all it can be clearly seen the pressure will at some point come close to stabilize, indicating a balance between incoming flow and reaction.

The final pressure was 0.43 bar, this pressure is used to calculate the increased resistance by Equation 29. Leading to a value for the total resistance of 2.89 x 10^{12}. The membrane resistance, Rm, of 8.97 x 10^9 is calculated in Chapter 4.2. Substracting the intrinsic membrane resistance from the total resistance leads to the resistance by fouling, Rf, of 1.99 x 10^{12}, which is 221 times higher than the intrinsic membrane resistance.

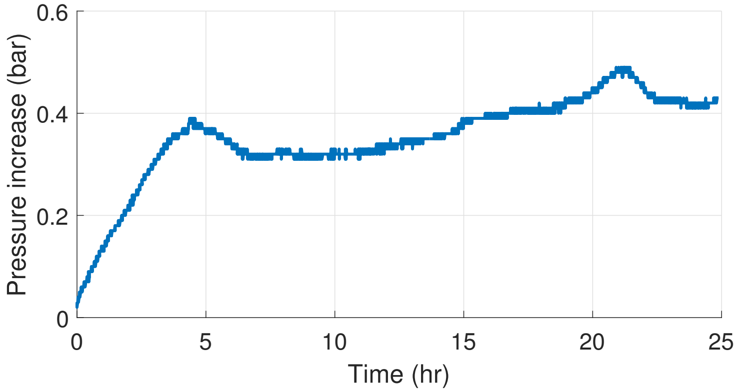

Figure 4.7: Pressure over time for an irridiated membrane filtration

4.4 Steady state experiments

Several experiments have been done similarly to the experiment in Chapter 4.3.2. Table 1 shows an overview of the final dimensionless concentrations, pressure, the membrane properties and system flowrate. This has only been done for the plasma oxidized membranes.

Table 1: Results for steady state experiments

Membrane	Diameter (mm)	Flowrate (g/hr)	Concentration (-)	TMP (bar)
A	4mm (x4)	0.5	0.14	0.10
B	4mm	0.5	0.44	0.41
B	4mm	0.2	0.24	0.22
C	3mm	0.5	0.28	0.77
C	3mm	0.2	0.25	0.68
D	2mm	0.4	0.23	0.72
D	2mm	0.2	0.22	0.43
D	2mm	0.1	0.21	0.26

Membrane A showed a great reduction of methylene blue, 86% of the total methylene blue concentration was either filtered or reacted by the photocatalytic membrane. Unfortunately the membrane had a small rupture in one of the holes, which made it unable to use anymore. Therefore only one experiment has been done with this membrane.
Membrane B shows a significant difference in concentration for the different flowrates 0.5 and 0.2 g/hr. This possibly happened due to the continuity of the experiments, the module was not opened and thus the membrane was not cleaned in between experiments.
Identically with membrane B, membrane C was not cleaned between experiments. However this time the 0.5 g/hr experiment was done before the 0.2 g/hr experiment. Even so the concentration decreased to nearly the same amount as membrane B, however the pressure did not drop significantly.
Membrane D was treated differently, the module was opened between the different experiments and the membrane was put in an oven to burn off all contaminents to clean the membrane. The membrane shows conversions of over 77% for all flowrates which have been used. The difference in conversion implies the likelyness of a difference in porosity between membrane B & D. The experiment with membrane B at 0.2 g/hr was done with a clean membrane. According to the mass transfer model the concentration is expected to be lower than the 0.2 g/hr experiment of membrane D, since a larger membrane surface area induces lower local velocities in membrane B.

Reproducing experiments has shown to be hard, unless membranes are cleaned in an oven. Leaving the membranes overnight in Isopropyl alcohol (IPA) did not clean the membranes properly. The fact that IPA was unable to clean the membranes, it can be assumed the membranes adsorp methylene blue on its surface and in its pores. For now, the only way to clean the membranes properly and thus be able to reproduce experiments is by treating the membranes in an oven to remove all contaminents.

4.5 Solving experimental data with respect to the mass transfer model

The values of the parameters as described in Chapter 4.4 can now be used to calculate the missing parameters; reaction rate constant, k, and the porosity, ϵ.These parameters have a great effect on the final concentration, thus conversion. Since all membranes use the same catalyst, it is assumed the reaction rate constant will be in the same order of magnitude for all membranes. It is known the porosities are ranged between 20 and 80% (given by Metal Membranes). This extensive range however, can make significant differences in conversion. For example; the difference in final concentration, for a membrane with a porosity of 20% and 80%, easily goes over a factor of 2.5.

Considering membrane D was cleaned in between its experiments, it will be taken to calculate the reaction rate constant. Besides, membrane D is the only membrane

with three results. Since there are three unknowns, three equations are required. Solving these equations leads to a porosity of 0.232, a membrane thickness of 66μm and a reaction rate constant of 0.065. As mentioned above, the reaction rate is assumed to be similar for all membranes. The 0.5 g/hr experiment for membrane B is discarded, its final value indicates there has been a problem with either the cleaning or measurement apparatus.
Solving all equations lead to the values given in Table 2.

Table 2: Calculated reaction rate constant and porosity

Membrane	Thickness (μm)	Porosity (-)	Reaction rate constant (1/s)
A	72	0.201	0.065
B	63	0.321	0.065
C	62	0.296	0.065
D	66	0.232	0.065

Remarkablly, a significant difference in porosities has been found. The porosity of membrane A appears to be 1.6 times lower than the membrane with the highest porosity, membrane B. The difference in membrane thickness is relatively smaller. The membrane (A) with the highest thickness is only 16% larger than the smallest membrane (C).

4.6 Sensitivity analysis

Some parameters have great effect on the final concentration of methylene blue and the Concentration polarization (CP) modulus, which can be calculated according to Equation 31. Therefore a sensitivity analysis has been done for these parameters. It is expected this sensitivity analysis will give insight in the effect of all parameters which can be controlled. Sensitivity analysis will be done for the following parameters; membrane surface area, membrane porosity and membrane thickness.

$$C_p = \frac{C_m}{C_b} \tag{31}$$

Where C_p is the dimensionless concentration polarization modulus, C_m the dimensionless surface concentration and C_b the dimensionless bulk concentration, which is equal to unity in the mass transfer model.

4.6.1 Relation CP-modulus and pressure

There appears to be a relation between the CP-modulus, which indicates the concentration at the membrane surface, and the required pressure of the system. As depicted in Figure 4.8, the pressure increases logarithmically with the CP-modulus.

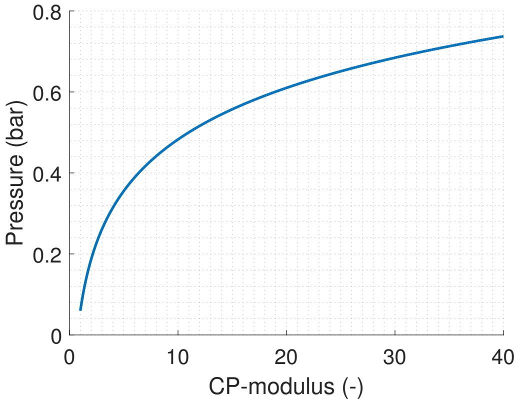

Figure 4.8: Pressure vs. CP-modulus based on results of membrane A & D in Table 1

4.6.2 Membrane surface area

A larger membrane surface area reduces the relative velocity in the membrane, which relates to higher converions. The membrane surface area will be examined for a minimum diameter of 2 mm and a maximum diameter of 2 cm, which is the limit of the photocatalytic membrane module. Of course the membrane surface area can be significantly larger when used in another module, or even other applications. Besides having a positive effect on the degredation of methylene blue, a larger surface area would also reduce the effects of concentration polarization which means it can achieve higher flowrates with an identical pressure. Figure 4.9 represents the dimensionless final concentratration and CP-modulus related to the membrane effective diameter in mm. For lower surface area's a small increase can result in a large increase of conversion. When going to larger surface area's however, the concentration will reduce less when increasing the surface area allthough it will still decrease. When going to very high surface area's the concentration will eventually come close to zero. When increasing the membrane surface area and keeping a stable flowrate, it lead to a fast paced reduction in concentration polarization for the lower regions. When the CP-modulus gets below one it means the equilibrium between reaction and retained species is in favor of the reaction. This would also lead to a reduction in pressure.

4.6.3 Membrane porosity

Membrane porosity has a great effect on the mass transfer within a membrane. Lower values of porosity will lead to higher velocity differences, and thus more filtration. Even so the porosity affects the effective diffusion as described in Chapter 3.4.1, leading to another difference in axial mass transfer between the bulk and the membrane. A lower porosity value corresponds with higher relative velocities and

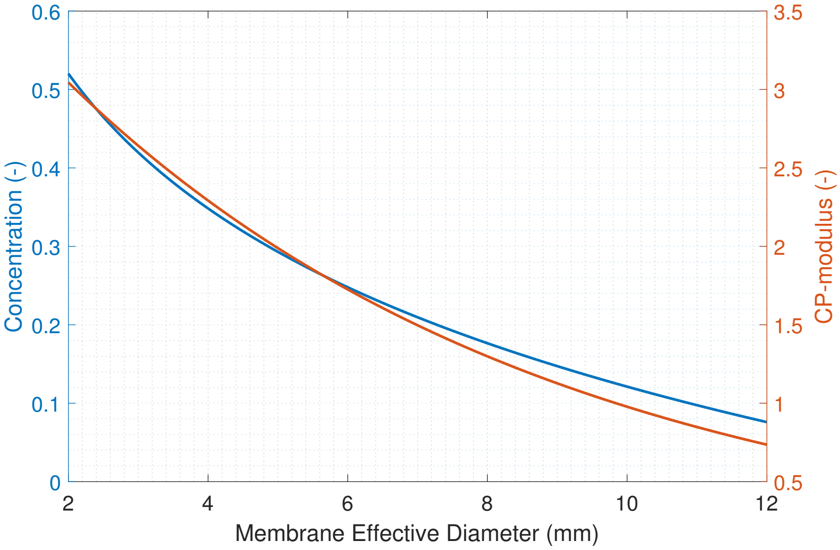

Figure 4.9: Dimensionless final concentration and CP-modulus vs. membrane surface area. Flowrate = 0.2 g/hr, Porosity = 0.25, Membrane thickness = 65 μm and $\alpha = 5$

diffusivities inside the membrane. Thus a low porosity reduces the final concentration but increases effects of concenstration polarization. Lower porosities lead to bigger differences in local velocities between the bulk and the membrane. Therefore more species are retained at low porosities, increasing the membrane concentration. Thus it increases the concentration polarization modulus. Figure 4.10 describes the dimensionless concentration and CP-modulus related to the porosity ranging from 0.2 to 0.8. As can be clearly seen, higher porosities lead to hgher final concentration. On the other hand it reduces the CP-modulus, which is related to the required pressure or flux due to its increasing fouling resistance. Lower porosities give better results, however the CP-modulus should not be forgotten.

4.6.4 Membrane thickness

The membrane thickness is an important parameter for photocatalytic membrane filtration. Increasing the membrane thickness leads to a longer residence time. Longer residence times for reactions result into higher conversions and thus a lower final concentration. On the other hand, increasing membrane thickness will also increase the membrane resistance and thus the required pressure for a system. Figure 4.11 represents the final dimensionless concentration and CP-modulus for a membrane thickness between 20 and 80 μm. Both the concentration and CP-modulus appear to decrease and increase linearly with an increasing membrane thickness. In reality however, the trend of the final concentration would most likely

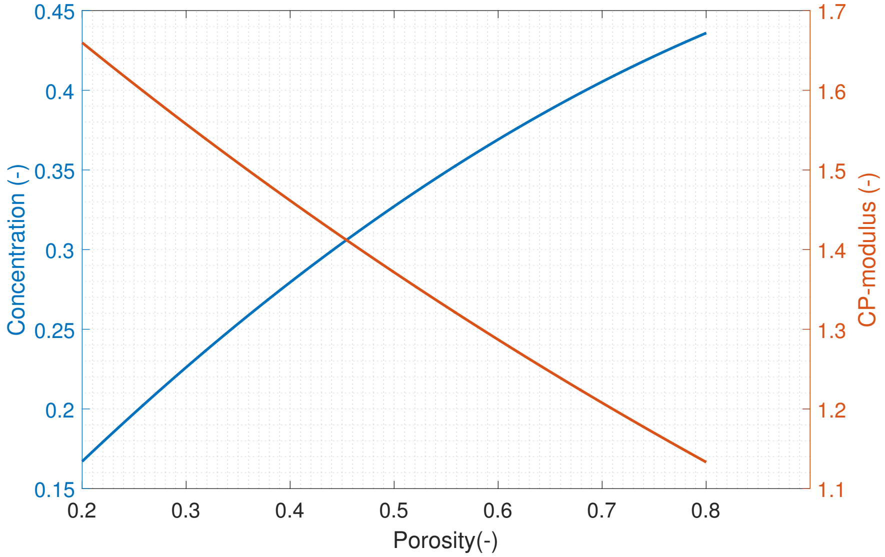

Figure 4.10: Dimensionless final concentration and CP-modulus vs. porosity. Flowrate = 0.2 g/hr, Membrane surface area = 0.13 cm^2, Membrane thickness = 65 μm and $\alpha = 5$

not be linear. For now, it is assumed the light intensity is equal over the entire thickness of the membrane. It is very unlikely this is really the case, especially for membranes in the thicker region.

4.7 Neglectig mass transfer

As described in Chapter 1.4.1, the pseudo-first order simplified equation of Langmuir-Hinshelwood is generally used to describe reaction rate constants in photocatalytic membrane reactions. When applying this equation to several experiments, a k-value in the order of 1 x $10^{-5}s^{-1}$ can be found.
As shown in Chapter 4.5, the reaction rate constant k for the mass transfer model used in this research gives a value in the order of 1 x $10^{-2}s^{-1}$. The significant difference between these values is due to implementing mass transfer equations, which also describe mass transfer effects besides the reaction kinetics.

4.8 Result overview

Unfortunately the experiments for the α-Al_2O_3 supported membranes were deemed unsuccessful. Electrospinning on an alumina support appeared to be ineffective due to not being able to create an uniform layer of TiO_2. On the other hand, sol dip coating was succesful in terms of creating an uniform layer of TiO_2 on the support.

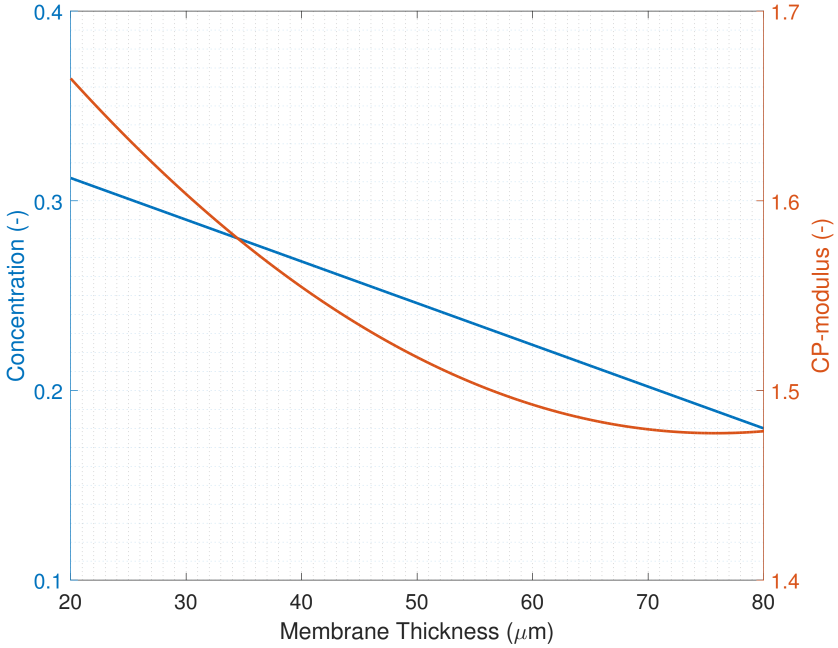

Figure 4.11: Dimensionless final concentration and CP-modulus vs. membrane thickness. Flowrate = 0.2 g/hr, Membrane surface area = 0.13 cm^2, Porosity = 0.25and $\alpha = 5$

Even so the support had to be cut to get the right dimensions for the photocatalytic membrane filtration module. This resulted in lower mechanical strength and breaking membranes for experiments including methylene blue.

A significant difference in intrinsic membrane resistance was acquired for the sol dip coated membranes and the plasma oxidated membranes. The compelling difference in membrane thickness was most likely the main cause for this difference in intrinsic membrane resistance. For both the intrinsic membrane resistance and membrane thickness, the alumina membranes had values of 400 and 346 times higher than the plasma oxidized membranes.

The plasma oxidized membranes gave a significant difference in pressure relations between irridiated and non-irridiated systems. The non-irridiated system, thus general dead-end membrane filtration gave a close to linear increase in pressure over time. This increase made pressure rise over the limits of the membranes, causing them to break. The irriated system showed similar results for the first hours of the experiments, except for the lower slope. After several hours the system stabilized and reached a stable pressure with some fluctuations.

Results of the steady state experiments for the plasma oxidized membranes showed a very low concentration for a high surface area membrane. Furthermore it showed slight differences in porosity or membrane thickness can have great effects on the final concentration an pressure. Conversions of up to 86% have been achieved in the photocatalytic membran reactor. It appeared to be hard to exactly reproduce the experiments, mostly due to cleaning. Leaving the membranes in IPA did not clean the membranes sufficiently. The only method to clean the membranes properly was by putting them into an oven for 10 h at 500 °C in air with heating and cooling steps of 2 °C/min.

Fitting the results into the mass transfer model gave a reaction rate constant of 0.065 s^{-1}. Even so a difference in thickness and porosity between membranes was observed. With a membrane thickness ranging from 62 to 72 μm and a porosity ranging from 0.201 to 0.321.

Relating the CP-modulus to the pressure and resistance gave intersting results. A higher CP-modulus related to a higher pressures, as expected. The resistance however, tended to decrease with the CP-modulus. Likely, this happened due to other resistances than R_{CP} in the lower regions of the CP-modulus, which also has a lower flux. For example resistances by pore blocking or adsorption.

Table 3: Overview sensitvity analysis

Parameter	**Influence concentration**	**Influence CP-modulus**
Membrane surface area	Negative logarithmic	Negative logarithmic
Porosity	Positive polynomial	Negative linear
Membrane thickness	Negative linear	Positive linear
Flowrate	Positive logarithmic	Positive exponential

The sensitivity analysis gave insight in the effect of several (controllable) parameters on the concentration and CP-modulus. Table 3 gives an overview of the sensitivity analysis.

The membrane surface area reduces both the final concentration and the CP-modulus, which is a positive result. A larger membrane surface area ensures a larger catalyst surface area, thus more reaction. This decreases the final concentration. On the other hand it also reduces the flux, which leads to less species permeating per surface area and hence a smaller CP-modulus. For larger membrane surface area's however, the reduction by increasing the membrane surface area gets smaller.

Increasing porosity has a negative effect on the final concentration, thus it increases. Higher porosity leads to less retention, which allows more solute to permeate trough

the membrane. For the same reason, a increasing porosity reduces the effect of concentration polarization.
The membrane thickness has linear effects for both the concentration as CP-modulus. By making the membrane thicker, the residence time of the species in the membrane increases which means they have more time to react. The assumption of a constant reaction rate over the thickness of the membrane may not be valid, which would in reality lead to a smaller slope for the thicker regions. Due to increasing membrane thickness, the resistance increases, which leads to higher values of concentration polarization.

5 Conclusions

Insight into a dead-end photocatalytic membrane has been aqcuired by applying a mass transfer model on experimental results. Optimization has led to a model which can predict the concentration profile in dead-end photocatalytic membrane filtration.

Steady-state experiments have been succesfully conducted, giving the difference in pressure increase (flux decline) between irridiated and non-irridiated systems.

Degradation of up to 86% of methylene blue has been achieved under the effect of irridiation, while applying relatively low pressures. Trans membrane pressures have remained below 1 bar for plasma oxidized TiO_2 membranes. α-Al_2O_3 supported membranes have shown to be unfit for this particular dead-end membrane reactor.

Differences in instrinsic membrane resistances between traditional supported membranes and plasma oxidized membranes have shown to be significant; a difference of up to 400 times the resistance.

Solving unknown parameters by relating experimental results to the model has acquired a reaction rate constant of 0.065 s^{-1}. Where models which generally use a first order plug flow reaction equation leading to results in the order of 1 x 10^-5s^{-1}.

Sensitivity analysis has provided the effects on the concentration profile and concentration polarization of important parameters such as membrane surface area, membrane porosity, membrane thickness and flowrate/flux.

All in all plasma oxidized membranes have shown great potential for photocatalytic membrane reactors, requiring less pressure and having higher reaction rates than supported membranes with a catalyst layer.

6 Recommendations & outlook

Several recommendations can be made for future research for photocatalytic membrane reactors. Also an outlook was made to describe the potential for industrial applications.

First of all, for future experiments it is advised to have the exact values of the available membranes. In this research both the membrane thickness and porosity had a relatively large range of variety. Knowing these parameters would lead to results which are easier to validate with a mass transfer model.

An important factor of reproducing results when re-using membranes is the cleaning of the membranes. For now, the only way to reproduce experiments was by cleaning them in an oven for 10 h at 500 °C in air with heating and cooling steps of 2 °C/min. As long as no other options are found to completely clean the membranes, it is recommended to use this method.

Increasing the membrane surface area of the plasma oxidized TiO_2 membranes can possibly be a great advantage. Currently the average diameter of the membranes was 4mm while the photocatalytic membrane module allows a diameter of 2cm. As shown in the sensitivity analysis increasing the membrane surface area relates to more degradation with less concentration polarization. This allows for higher flowrates with relative low pressures. One of the main problems with the small area membranes was the limited pressure they could handle before breaking.

Additionally it can be of great value to validate the results of the sensitivity analysis experimentally. If porosity and membrane thickness can be controlled more closely than they are now, complete validation of the mass transfer model would be possible.

In this research the effect of the light intensity was not evaluated. There is a possibility however, that the light intensity affects the reaction rate constant. Moreover, it is assumed the reaction rate remains constant over the entire thickness of the membrane. The light intenstiy is highly likely to be reducing over the length of the membrane and if the light intensity affects the reaction rate, this would mean the reaction rate also decreases over the length of the membrane.

Furthermore it is advised to change from dead-end to cross-flow filtration. With cross-flow it would be easier to increase the irridiated surface area of the module since the solvent does not originate from the same direction as the UV-light. Cross-flow allows for UV-light sources perpendicular to the membrane surface. On top of this, cross-flow filtration has more possibilities in possible future industrial applications since it allows insoluble materials and viscous liquids in the waste stream.

In this research, plasma oxidized TiO_2 membranes have shown great potential. Eventually photocatalytic membrane module containing plasma oxidized membranes could be used for industrial purposes to either purify water or destroy bacteria. It could be scaled up by putting several modules in paralel or by possibly increased dimensions of the photocatalytic membrane reactors. Even if one module does not meet the specifications for the purified water, another set of modules could be put in series.

References

[1] W.-Y. Wang, A. Irawan, and Y. Ku, "Photocatalytic degradation of acid red 4 using a titanium dioxide membrane supported on a porous ceramic tube," *Water Research*, vol. 42, no. 19, pp. 4725–4732, 2008.

[2] S. Yang, J.-S. Gu, H.-Y. Yu, J. Zhou, S.-F. Li, X.-M. Wu, and L. Wang, "Polypropylene membrane surface modification by raft grafting polymerization and tio2 photocatalysts immobilization for phenol decomposition in a photocatalytic membrane reactor," *Separation and Purification Technology*, vol. 83, pp. 157–165, 2011.

[3] S. Leong, A. Razmjou, K. Wang, K. Hapgood, X. Zhang, and H. Wang, "Tio2 based photocatalytic membranes: A review," *Journal of Membrane Science*, vol. 472, pp. 167–184, 2014.

[4] N. M. Mahmoodi, M. Arami, and N. Y. Limaee, "Photocatalytic degradation of triazinic ring-containing azo dye (reactive red 198) by using immobilized tio2 photoreactor: Bench scale study," *Journal of Hazardous Materials*, vol. 133, no. 13, pp. 113–118, 2006.

[5] H. A. Le, L. T. Linh, S. Chin, and J. Jurng, "Photocatalytic degradation of methylene blue by a combination of tio2-anatase and coconut shell activated carbon," *Powder Technology*, vol. 225, pp. 167–175, 2012.

[6] R. Mu, Z. Xu, L. Li, Y. Shao, H. Wan, and S. Zheng, "On the photocatalytic properties of elongated tio2 nanoparticles for phenol degradation and cr(vi) reduction," *Journal of Hazardous Materials*, vol. 176, no. 13, pp. 495–502, 2010.

[7] Z. Miao, S. Tao, Y. Wang, Y. Yu, C. Meng, and Y. An, "Hierarchically porous silica as an efficient catalyst carrier for high performance vis-light assisted fenton degradation," *Microporous and Mesoporous Materials*, vol. 176, pp. 178–185, 2013.

[8] S. Liu, X. Wang, W. Zhao, K. Wang, H. Sang, and Z. He, "Synthesis, characterization and enhanced photocatalytic performance of ag2s-coupled zno/zns core/shell nanorods," *Journal of Alloys and Compounds*, vol. 568, pp. 84–91, 2013.

[9] H. Zhang, X. Quan, S. Chen, H. Zhao, and Y. Zhao, "Fabrication of photocatalytic membrane and evaluation its efficiency in removal of organic pollutants from water," *Separation and Purification Technology*, vol. 50, no. 2, pp. 147–155, 2006.

[10] C. P. Athanasekou, G. E. Romanos, F. K. Katsaros, K. Kordatos, V. Likodimos, and P. Falaras, "Very efficient composite titania membranes in hybrid ultrafiltration/photocatalysis water treatment processes," *Journal of Membrane Science*, vol. 392393, pp. 192–203, 2012.

[11] L. Djafer, A. Ayral, and A. Ouagued, “Robust synthesis and performance of a titania-based ultrafiltration membrane with photocatalytic properties,” *Separation and Purification Technology*, vol. 75, no. 2, pp. 198–203, 2010.

[12] A. Alem, H. Sarpoolaky, and M. Keshmiri, “Titania ultrafiltration membrane: Preparation, characterization and photocatalytic activity,” *Journal of the European Ceramic Society*, vol. 29, no. 4, pp. 629–635, 2009.

[13] W.-Y. Choi, J. Chung, C.-H. Cho, and J.-O. Kim, “Fabrication and photocatalytic activity of a novel nanostructured tio2 metal membrane,” *Desalination*, vol. 279, no. 13, pp. 359–366, 2011.

[14] H. Choi, S. R. Al-Abed, D. D. Dionysiou, E. Stathatos, and P. Lianos, *Chapter 8 TiO2-Based Advanced Oxidation Nanotechnologies for Water Purification and Reuse*, vol. Volume 2, pp. 229–254. Elsevier, 2010.

[15] Z. Liu, X. Zhang, S. Nishimoto, M. Jin, D. A. Tryk, T. Murakami, and A. Fujishima, “Highly ordered tio2 nanotube arrays with controllable length for photoelectrocatalytic degradation of phenol,” *The Journal of Physical Chemistry C*, vol. 112, no. 1, pp. 253–259, 2008.

[16] S. Mozia, “Photocatalytic membrane reactors (pmrs) in water and wastewater treatment. a review,” *Separation and Purification Technology*, vol. 73, no. 2, pp. 71–91, 2010.

[17] D. J. Miller, S. Kasemset, D. R. Paul, and B. D. Freeman, “Comparison of membrane fouling at constant flux and constant transmembrane pressure conditions,” *Journal of Membrane Science*, vol. 454, pp. 505–515, 2014.

[18] R. W. Field, D. Wu, J. A. Howell, and B. B. Gupta, “Critical flux concept for microfiltration fouling,” *Journal of Membrane Science*, vol. 100, no. 3, pp. 259–272, 1995.

[19] G. B. van den Berg and C. A. Smolders, “Flux decline in ultrafiltration processes,” *Desalination*, vol. 77, pp. 101–133, 1990.

[20] P. Bacchin, P. Aimar, and R. W. Field, “Critical and sustainable fluxes: Theory, experiments and applications,” *Journal of Membrane Science*, vol. 281, no. 12, pp. 42–69, 2006.

[21] R. Molinari, C. Lavorato, and P. Argurio, “Recent progress of photocatalytic membrane reactors in water treatment and in synthesis of organic compounds. a review,” *Catalysis Today*, vol. 281, Part 1, pp. 144–164, 2017.

[22] W. Zhang, L. Ding, J. Luo, M. Y. Jaffrin, and B. Tang, “Membrane fouling in photocatalytic membrane reactors (pmrs) for water and wastewater treatment: A critical review,” *Chemical Engineering Journal*, vol. 302, pp. 446–458, 2016.

[23] M. N. Chong, B. Jin, C. W. K. Chow, and C. Saint, “Recent developments in photocatalytic water treatment technology: A review,” *Water Research*, vol. 44, no. 10, pp. 2997–3027, 2010.

[24] S. O. Ganiyu, E. D. van Hullebusch, M. Cretin, G. Esposito, and M. A. Oturan, "Coupling of membrane filtration and advanced oxidation processes for removal of pharmaceutical residues: A critical review," *Separation and Purification Technology*, vol. 156, Part 3, pp. 891–914, 2015.

[25] N. Ma, X. Fan, X. Quan, and Y. Zhang, "Agtio2/hap/al2o3 bioceramic composite membrane: Fabrication, characterization and bactericidal activity," *Journal of Membrane Science*, vol. 336, no. 12, pp. 109–117, 2009.

[26] S. H. Kim, S.-Y. Kwak, B.-H. Sohn, and T. H. Park, "Design of tio2 nanoparticle self-assembled aromatic polyamide thin-film-composite (tfc) membrane as an approach to solve biofouling problem," *Journal of Membrane Science*, vol. 211, no. 1, pp. 157–165, 2003.

[27] S.-J. You, G. U. Semblante, S.-C. Lu, R. A. Damodar, and T.-C. Wei, "Evaluation of the antifouling and photocatalytic properties of poly(vinylidene fluoride) plasma-grafted poly(acrylic acid) membrane with self-assembled tio2," *Journal of Hazardous Materials*, vol. 237238, pp. 10–19, 2012.

[28] P. Liu, H. Liu, G. Liu, K. Yao, and W. Lv, "Preparation of tio2 nanotubes coated on polyurethane and study of their photocatalytic activity," *Applied Surface Science*, vol. 258, no. 24, pp. 9593–9598, 2012.

[29] J. Liao, S. Lin, N. Pan, S. Li, X. Cao, and Y. Cao, "Fabrication and photocatalytic properties of free-standing tio2 nanotube membranes with through-hole morphology," *Materials Characterization*, vol. 66, pp. 24–29, 2012.

[30] L. Liu, Z. Liu, H. Bai, and D. D. Sun, "Concurrent filtration and solar photocatalytic disinfection/degradation using high-performance ag/tio2 nanofiber membrane," *Water Research*, vol. 46, no. 4, pp. 1101–1112, 2012.

[31] A. Hu, X. Zhang, K. D. Oakes, P. Peng, Y. N. Zhou, and M. R. Servos, "Hydrothermal growth of free standing tio2 nanowire membranes for photocatalytic degradation of pharmaceuticals," *Journal of Hazardous Materials*, vol. 189, no. 12, pp. 278–285, 2011.

[32] Y.-F. Lin, K.-L. Tung, Y.-S. Tzeng, J.-H. Chen, and K.-S. Chang, "Rapid atmospheric plasma spray coating preparation and photocatalytic activity of macroporous titania nanocrystalline membranes," *Journal of Membrane Science*, vol. 389, pp. 83–90, 2012.

[33] R. A. Damodar, S.-J. You, and H.-H. Chou, "Study the self cleaning, antibacterial and photocatalytic properties of tio2 entrapped pvdf membranes," *Journal of Hazardous Materials*, vol. 172, no. 23, pp. 1321–1328, 2009.

[34] R. Molinari, F. Pirillo, M. Falco, V. Loddo, and L. Palmisano, "Photocatalytic degradation of dyes by using a membrane reactor," *Chemical Engineering and Processing: Process Intensification*, vol. 43, no. 9, pp. 1103–1114, 2004.

[35] G. E. Romanos, C. P. Athanasekou, F. K. Katsaros, N. K. Kanellopoulos, D. D. Dionysiou, V. Likodimos, and P. Falaras, "Double-side active tio2-modified nanofiltration membranes in continuous flow photocatalytic reactors for effective water purification," *Journal of Hazardous Materials*, vol. 211212, pp. 304–316, 2012.

[36] X. Zhang, A. J. Du, P. Lee, D. D. Sun, and J. O. Leckie, "Tio2 nanowire membrane for concurrent filtration and photocatalytic oxidation of humic acid in water," *Journal of Membrane Science*, vol. 313, no. 12, pp. 44–51, 2008.

[37] L. Liu, F. Chen, and F. Yang, "Stable photocatalytic activity of immobilized fe0/tio2/acf on composite membrane in degradation of 2,4-dichlorophenol," *Separation and Purification Technology*, vol. 70, no. 2, pp. 173–178, 2009.

[38] F. Bosc, A. Ayral, and C. Guizard, "Mesoporous anatase coatings for coupling membrane separation and photocatalyzed reactions," *Journal of Membrane Science*, vol. 265, no. 12, pp. 13–19, 2005.

[39] H. Choi, E. Stathatos, and D. D. Dionysiou, "Photocatalytic tio2 films and membranes for the development of efficient wastewater treatment and reuse systems," *Desalination*, vol. 202, no. 1, pp. 199–206, 2007.

[40] H.-J. Hong, S. K. Sarkar, and B.-T. Lee, "Formation of tio2 nano fibers on a micro-channeled al2o3zro2/tio2 porous composite membrane for photocatalytic filtration," *Journal of the European Ceramic Society*, vol. 32, no. 3, pp. 657–663, 2012.

[41] A. Alem, H. Sarpoolaky, and M. Keshmiri, "Solgel preparation of titania multilayer membrane for photocatalytic applications," *Ceramics International*, vol. 35, no. 5, pp. 1837–1843, 2009.

[42] A. Alem and H. Sarpoolaky, "The effect of silver doping on photocatalytic properties of titania multilayer membranes," *Solid State Sciences*, vol. 12, no. 8, pp. 1469–1472, 2010.

[43] A. Rahimpour, M. Jahanshahi, B. Rajaeian, and M. Rahimnejad, "Tio2 entrapped nano-composite pvdf/spes membranes: Preparation, characterization, antifouling and antibacterial properties," *Desalination*, vol. 278, no. 1, pp. 343–353, 2011.

[44] X. Lu, M. Mohedano, C. Blawert, E. Matykina, R. Arrabal, K. U. Kainer, and M. L. Zheludkevich, "Plasma electrolytic oxidation coatings with particle additions a review," *Surface and Coatings Technology*, vol. 307, Part C, pp. 1165–1182, 2016.

[45] D. Li and Y. Xia, "Fabrication of titania nanofibers by electrospinning," *Nano Letters*, vol. 3, no. 4, pp. 555–560, 2003.

[46] E. Formo, E. Lee, D. Campbell, and Y. Xia, "Functionalization of electrospun tio2 nanofibers with pt nanoparticles and nanowires for catalytic applications," *Nano Letters*, vol. 8, no. 2, pp. 668–672, 2008.

[47] D. S. Gomes, A. N. R. d. Silva, N. I. Morimoto, L. T. F. Mendes, R. Furlan, and I. Ramos, "Characterization of an electrospinning process using different pan/dmf concentrations," *Polmeros*, vol. 17, pp. 206–211, 2007.

[48] A. Visan, D. Rafieian, W. Ogieglo, and R. G. H. Lammertink, "Modeling intrinsic kinetics in immobilized photocatalytic microreactors," *Applied Catalysis B: Environmental*, vol. 150151, pp. 93–100, 2014.

[49] H. C. Aran, D. Salamon, T. Rijnaarts, G. Mul, M. Wessling, and R. G. H. Lammertink, "Porous photocatalytic membrane microreactor (p2m2): A new reactor concept for photochemistry," *Journal of Photochemistry and Photobiology A: Chemistry*, vol. 225, no. 1, pp. 36–41, 2011.

[50] F. Bosc, A. Ayral, P.-A. Albouy, and C. Guizard, "A simple route for low-temperature synthesis of mesoporous and nanocrystalline anatase thin films," *Chemistry of Materials*, vol. 15, no. 12, pp. 2463–2468, 2003.

[51] C. J. Brinker, G. C. Frye, A. J. Hurd, and C. S. Ashley, "Fundamentals of sol-gel dip coating," *Thin Solid Films*, vol. 201, no. 1, pp. 97–108, 1991.

[52] Y. A. Makhnovskii, A. M. Berezhkovskii, and V. Y. Zitserman, "Diffusion in a tube of alternating diameter," *Chemical Physics*, vol. 367, no. 2, pp. 110–114, 2010.

A Appendix

A.1 Calculating integration constants

```
clear all;
clc;
close all;

syms A1 A2 A3 A4 m1 m2 Pe_1 Pe_2 B alpha D1 D2 u1 u2 L1 L2

eqn1 = A1+A2*exp(Pe_1*-B) == 1;
eqn2 = (D1/L2)*Pe_1*A2 - u1*(A1+A2) == (D2/L2)*(m1*A3+m2*A4) - u2*(A3+A4);
eqn3 = (A3+A4) == (A1+A2)/alpha ;
eqn4 = (m1*A3*exp(m1) + m2*A4*exp(m2))== 0;

[A,B] = equationsToMatrix([eqn1, eqn2, eqn3, eqn4], [A1 A2 A3 A4]);

Xnew = solve([eqn1,eqn2,eqn3,eqn4],[A1 A2 A3 A4]);
X(1) = Xnew.A1;
X(2) = Xnew.A2;
X(3) = Xnew.A3;
X(4) = Xnew.A4;
```

A.2 Solving concentration profile

```
%Define constants
F1 = 0.5;                       %Flowrate (g/hr)

rad = 0.001;                    %Radius membrane (m)
Area = rad^2*pi;                %Surface area membrane (m^2)

P = 0.232;                      %Porosity
u1 = (F1*(1e-6/3600))/Area;     %Velocity pre-membrane (m/s)
u2 = (F1*(1e-6/3600))/(Area*P); %Velocity in membrane (m/s) Asuuming cylindrical pores
D1 = 5.7e-10;                   %Diffusion coefficient pre-membrane (m2/s)
D2 = D1*P;                      %Diffusion coefficient membrane (m2/s)
L2 = 6.6e-5;                    %Membrane thickness  (m)
k = 0.065;                      %Reaction rate constant  (1/s)
K = L2^2*k/D2;                  %Damkohler number
L1 = 100e-5 ;                   %Mass transfer boundary layer (m)
B = L1/L2;                      %Mass transfer boundary/membrane thickness(-)
E0 = 0.01;                      %Enrichment factor (-)
Da = k*L2/u2;                   %Damkohler constant

Pe_1 = u1*L2/D1;
Pe_2 = u2*L2/D2;

Cs2 = (exp(Pe_1))/(1+E0*(exp(Pe_1)-1));      %CP-modulus(-)
alpha = Cs2/P;                               %Retention Factor (-)

m1 = 1/2*(Pe_2+sqrt(Pe_2^2+4*K));
m2 = 1/2*(Pe_2-sqrt(Pe_2^2+4*K));
```

```
x = -B:0.0001:1;
x1 = x(x>=-B & x<=0);
x2 = x(x>=0 & x<=1);

B1 = X(1);
B2 = X(2);
B3 = X(3);
B4 = X(4);

Q1 = simplify(B1);
Q2 = simplify(B2);
Q3 = simplify(B3);
Q4 = simplify(B4);

A1 = eval(B1);
A2 = eval(B2);
A3 = eval(B3);
A4 = eval(B4);

c1 = A1+A2*exp(Pe_1*x1);
c2 = A3*exp(m1*x2) + A4*exp(m2*x2);


width = 4;     % Width in inches
height = 4;    % Height in inches
alw = 0.75;    % AxesLineWidth
lw = 1.5;        % LineWidth
msz = 8;       % MarkerSize
tau=L2/u2;
lambda = Pe_2^2 -4*K;
c1(end) %CP-modulus
c2(end) %Final concentration
display(K)
display(Da)
display(Pe_2)
display(tau)
display(lambda)
Dx = (c1(1,1))/(c1(1,2))

%Plot Figure conc
figure(3); clf;
hold on
set(gca, 'FontSize', 15)
plot([x1], [c1], '-b', [x2],[c2], '-r',[0 0],[c1(end) c2(1)],'--g','LineWidth',lw,'MarkerSize',msz);
axis([-B 1 0 3])
grid on
xlabel('Dimensionless axial coordinate X = x/L2');
ylabel({'Dimensionless concentration';'C'});
legend('Concentration pre-membrane','Concentration in membrane','Rejection by filtration','Location',

% Save the file as EPS
% print('filtration','-depsc');


%Plot Figure reaction rate
figure(4); clf;
hold on
```

```
set(gca, 'FontSize', 10)
plot([x1], [0*c1], '-b', [x2],[K*c2], '-r',[0 0],[0*c1(end) K*c2(1)],'--g','LineWidth',lw,'MarkerSize
axis([-1 1 0 5])
grid on
xlabel('Dimensionless axial coordinate X = x/L2');
ylabel({'Dimensionless reaction';'K*C'});
legend('Concentration pre-membrane','Concentration in membrane','Rejection by filtration','Location',
```